SIAM J. SCI. COMPUT.
Vol. 42, No. 5, pp. B1173–B1192

NUMERICAL SOLUTION OF A LINEARIZED TRAVEL TIME TOMOGRAPHY PROBLEM WITH INCOMPLETE DATA*

MICHAEL V. KLIBANOV†, THUY T. LE‡, AND LOC H. NGUYEN‡

Abstract. We propose a new numerical method to solve the linearized problem of the travel time tomography with incomplete data. Our method is based on the technique of the truncation of the Fourier series with respect to a special basis of L^2. This way we derive a boundary value problem for a system of coupled PDEs of the first order. This problem is solved by the quasi-reversibility method. The spatially dependent Fourier coefficients of the solution to the linearized eikonal equation are obtained this way. Numerical results for highly noisy data are presented.

Key words. linearization, inverse kinematic problem, travel time tomography, numerical solution, convergence

AMS subject classifications. 35R25, 35R30

DOI. 10.1137/19M1299487

1. Introduction.

In this paper we develop a new numerical method for the linearized travel time tomography problem (TTTP) for the $d-$D case. Our data are both nonredundant and incomplete. Using results of [32], we establish the convergence of our method. In addition, we provide results of numerical experiments in the two-dimentional (2D) case. In particular, we demonstrate that our method provides good accuracy of images of complicated objects with 5% noise in the data. Furthermore, a satisfactory accuracy of images is demonstrated even for very high levels of noise between 80% and 170%.

In fact, both the idea of our method and source/detector configuration are close to those of our recent works [16, 32]. However, our case is a substantially more difficult one since the waves in our case propagate along geodesic lines rather than a radiation propagating along straight lines in [16, 32]. Still, although we formulate here results related to the convergence of our method, we do not prove them. The reason is that, as it turns out, proofs are very similar to those in [32]. In other words, surprisingly, the analytical apparatus of the convergence theory developed in [32] works well for the problem considered in this paper.

In the isotropic case of acoustic/seismic wave propagation, the TTTP is the problem of the recovery of the spatially distributed speed of propagation of acoustic/seismic waves from the first times of arrival of those waves. In the electromagnetic case this is the problem of the recovery of the spatially distributed dielectric constant from those times. Another name for the TTTP is the inverse kinematic problem (IKP). Waves are originated by some sources located either at the boundary of the closed bounded domain of interest or outside of this domain. Times of first arrival

*Submitted to the journal's Computational Methods in Science and Engineering section November 13, 2019; accepted for publication (in revised form) July 8, 2020; published electronically September 23, 2020.

https://doi.org/10.1137/19M1299487

Funding: This work was supported by U.S. Army Research Laboratory and U.S. Army Research Office grant W911NF-19-1-0044.

†Corresponding author. Department of Mathematics and Statistics, University of North Carolina at Charlotte, Charlotte, NC 28223 (mklibanv@uncc.edu).

‡Department of Mathematics and Statistics, University of North Carolina at Charlotte, Charlotte, NC 28223 (tle55@uncc.edu, loc.nguyen@uncc.edu).

from those sources are measured on a part of the boundary of that domain. The TTTP has well-known applications in geophysics; see, e.g., Romanov [28, Chapter 3].

The pioneering papers about the solution of the 1D TTTP were published by Herglotz [5] (1905) and then by Wiechert and Zoeppritz [36] (1907). Their method is described in Romanov [28, section 3 of Chapter 3]. It was recently discovered that, in addition to geophysics, the IKP has applications in the phaseless inverse scattering problem [17, 18, 29].

The next natural question after the classical 1D case of [5, 36] was about 2D and 3D cases. The first uniqueness and Lipschitz stability result for the 2D case was obtained by Mukhometov [23]; also see [1, 26]. Next, these results were obtained by Mukhometov and Romanov for the 3D case in [24, 28]. We also refer to the work of Stefanov, Uhlmann, and Vasy [33] for a more recent publication for the 3D case. As to the numerical methods for the inverse kinematic problem, we refer the reader to [30] for the 2D case and to [38] for the 3D case.

In all past publications about the IKP, the data are redundant in the 3D case and complete in both 2D and 3D cases. In two recent works of the first author [12, 13] two globally convergent numerical methods for the 3D TTTP with nonredundant incomplete data were developed.

Along with the full IKP, a significant applied interest is also in a linearized IKP; see [28, Chapter 3]. Below $d \geq 2$ is the dimension of the space $\mathbb{R}^d$. Points of this space are denoted as $\mathbf{x} \in \mathbb{R}^d$. Let $\overline{c} \equiv const. > 0$ be the speed of sound in a certain reference medium in $\mathbb{R}^d$, which we do not specify, and $c(\mathbf{x}) > 0$ be the variable speed of sound. Then the refractive index is [28, Chapter 3]

$$\mathbf{n}(\mathbf{x}) = \overline{c}/c(\mathbf{x}). \tag{1.1}$$

To linearize, one should assume that $\mathbf{n}(\mathbf{x}) = \mathbf{n}_0(\mathbf{x}) + \mathbf{n}_1(\mathbf{x})$, where $\mathbf{n}_0(\mathbf{x})$ is the known background function and $\mathbf{n}_1(\mathbf{x})$ with $|\mathbf{n}_1(\mathbf{x})| \ll \mathbf{n}_0(\mathbf{x})$ is its unknown perturbation, which is the subject to the solution of the linearized TTTP. Thus, one assumes that the refractive index is basically known, whereas its small perturbation $\mathbf{n}_1$ is unknown. This problem is also called the *geodesic X-ray transform problem*. The Lipschitz stability and uniqueness theorem for this problem in the isotropic case was first obtained in [27]; see Theorem 3.2 in section 4 of Chapter 3 of [28]. In the nonisotropic case this problem was studied in [34]. In [22] numerical studies of this problem in the isotropic case were performed.

In our derivation, we end up with an overdetermined boundary value problem for a system of coupled linear PDEs of the first order. It is well known that the quasi-reversibility method is an effective tool for numerical solutions of overdetermined boundary value problems for PDEs. Lattès and Lions [19] were the first ones who proposed the quasi-reversibility method. This technique was developed further in, e.g., [2, 3, 6, 10, 16, 21, 32]. In particular, it was shown in [10] that while it is rather easy to prove, using the Riesz theorem, the existence and uniqueness of the minimizer of a certain functional related to this method, the proof of convergence of those minimizers to the correct solution requires a stronger tool of Carleman estimates.

Another important feature of this paper is a special orthonormal basis in the space $L^2(-\overline{\alpha}, \overline{\alpha})$, where $\overline{\alpha} > 0$ is a certain number. The functions of this basis depend only on the position of the point source. This basis was first introduced in [11] and was further used in [9, 12, 14, 13, 15, 16, 20, 32]. Just like in these previous publications, we use here an *approximate mathematical model*. More precisely, we assume that a certain function associated with the solution of the governing linearized eikonal equation can be represented via a truncated Fourier series with respect to this basis.

This assumption forms the first element of that model. The second element is that we assume that the first derivatives with respect to all variables are written via finite differences and that the step size of these finite differences with respect to all variables, except of one, is bounded from below by a positive number $h_0 > 0$.

We do not prove convergence for the case when $h_0 \to 0^+$ and the number N of terms in that truncated series tends to infinity. Thus, we come up with a finite dimensional approximate mathematical model. We point out that similar approximate mathematical models are used quite often in studies of numerical methods for inverse problems, and numerical results are usually encouraging; see, e.g., [4, 8, 7, 14, 32, 37]. Just as shown here, proof of convergence results in such cases when, e.g., $N \to \infty, h_0 \to 0^+$ are usually not conducted since they are very challenging tasks due to the ill-posed nature of inverse problems.

The paper is organized as follows. In section 2, we formulate the inverse problem. Next, in section 3, we introduce the truncation technique and our numerical method. Then, in section 4, we recall the quasi-reversibility method and its convergence in the case of partial finite differences. In section 5, we present the implementation and numerical results. Finally, section 6 is for concluding remarks.

2. The linearization. Consider numbers R, a, b such that $R > 1$ and $0 < a < b$. Set

$$\Omega = (-R, R)^{d-1} \times (a, b) \subset \mathbb{R}^d. \tag{2.1}$$

Recall that by (1.1) $\mathbf{n}(\mathbf{x}) = \overline{c}/c(\mathbf{x})$, where $c(\mathbf{x})$ is the speed of sound propagation and $n(\mathbf{x})$ is the refractive index. Let the function $\mathbf{n}_0(\mathbf{x})$ be the known refractive index of the background. We assume that

$$\mathbf{n}_0, \mathbf{n} \in C^2\left(\mathbb{R}^d\right);\ \mathbf{n}_0^2(\mathbf{x}), \mathbf{n}^2(\mathbf{x}) \geq 1 \text{ in } \Omega, \tag{2.2}$$

$$\mathbf{n}_0^2(\mathbf{x}) = \mathbf{n}^2(\mathbf{x}) = 1 \text{ for } \mathbf{x} \in \mathbb{R}^d \setminus \Omega. \tag{2.3}$$

For any two points $\mathbf{x}_1$ and $\mathbf{x}_2$ in $\mathbb{R}^d$, define the geodesic line generated by $\mathbf{n}_0$ connecting $\mathbf{x}_1$ and $\mathbf{x}_2$ as

$$\Gamma_0(\mathbf{x}_1, \mathbf{x}_2) = \operatorname{argmin}\Big\{ \int_\gamma \mathbf{n}_0(\boldsymbol{\xi}) d\sigma(\boldsymbol{\xi}), \text{ where } \gamma : [0,1] \to \mathbb{R}^d \text{ is a smooth map with } \gamma(0) = \mathbf{x}_1, \gamma(1) = \mathbf{x}_2 \Big\}. \tag{2.4}$$

Here, $d\sigma(\xi)$ is the elementary arc length. Note that by (2.4) the geodesic line $\Gamma_0(\mathbf{x}_1, \mathbf{x}_2)$ connects points $\mathbf{x}_1$ and $\mathbf{x}_2$. Let

$$\mathbf{a}_0(\mathbf{x}) = \mathbf{n}_0^2(\mathbf{x}) \quad \text{for all } \mathbf{x} \in \mathbb{R}^d. \tag{2.5}$$

The corresponding travel time between $\mathbf{x}_1$ and $\mathbf{x}_2$ is the integral

$$\int_{\Gamma_0(\mathbf{x}_1, \mathbf{x}_2)} \mathbf{n}_0(\boldsymbol{\xi}) d\sigma(\boldsymbol{\xi}) = \int_{\Gamma_0(\mathbf{x}_1, \mathbf{x}_2)} \sqrt{\mathbf{a}_0(\boldsymbol{\xi})} d\sigma(\boldsymbol{\xi}).$$

Introduce the line of sources L_s located on the x_1-axis as

$$L_s = [-\overline{\alpha}, \overline{\alpha}] \times \{(0, 0, \dots, 0)\}, \tag{2.6}$$

where $\overline{\alpha}$ is a fixed positive number. It follows from (2.1) and (2.6) that

$$\overline{\Omega} \cap L_s = \varnothing. \tag{2.7}$$

For $\mathbf{x}_\alpha \in L_s$, the travel time along $\Gamma_0(\mathbf{x}, \mathbf{x}_\alpha)$ of the wave from $\mathbf{x}_\alpha$ to $\mathbf{x}$ is

$$u_0(\mathbf{x}, \mathbf{x}_\alpha) = \int_{\Gamma_0(\mathbf{x}, \mathbf{x}_\alpha)} \sqrt{\mathbf{a}_0(\boldsymbol{\xi})} d\sigma(\boldsymbol{\xi}), \quad \mathbf{x} \in \mathbb{R}^d. \tag{2.8}$$

Assumption 2.1 (regularity of geodesic lines). We assume everywhere in this paper that the geodesic lines are regular in the following sense: For each point $\mathbf{x}$ of the closed domain $\overline{\Omega}$ and for each point $\mathbf{x}_\alpha$ of the line of sources L_s there exists a single geodesic line $\Gamma_0(\mathbf{x}, \mathbf{x}_\alpha)$ connecting them.

The inverse problem we consider arises from the highly nonlinear and severely ill-posed inverse kinematic problem. We now present the formal linearization arguments in exactly the same way as they are presented in Romanov [28, section 4 of Chapter 3]. Just as in [28], we avoid a setting via functional spaces for brevity.

Assume that the function $\mathbf{a}(\mathbf{x}) = \mathbf{n}^2(\mathbf{x})$ contains a perturbation term of the background function $\mathbf{a}_0(\mathbf{x}) = \mathbf{n}_0^2(\mathbf{x})$. In other words,

$$\mathbf{a}(\mathbf{x}) = \mathbf{a}_0(\mathbf{x}) + 2\epsilon \sqrt{\mathbf{a}_0(\mathbf{x})} p(\mathbf{x}), \quad \mathbf{x} \in \mathbb{R}^d, \tag{2.9}$$

where $\epsilon > 0$ is a sufficiently small number. Here, the function $p \in C\left(\mathbb{R}^d\right)$ and $p\left(\mathbf{x}\right) = 0$ for $\mathbf{x} \notin \overline{\Omega}$. Hence, by (2.7), $p(\mathbf{x}) = 0$ for points $\mathbf{x}$ in a small neighborhood of the line of sources L_s. Denote

$$u_{\mathbf{n}}(\mathbf{x}, \mathbf{x}_\alpha) = \int_{\Gamma_{\mathbf{n}}(\mathbf{x}, \mathbf{x}_\alpha)} \mathbf{n}(\boldsymbol{\xi}) d\sigma(\boldsymbol{\xi})$$

the travel time from the point $\mathbf{x}_\alpha \in L_s$ to the point $\mathbf{x} \in \Omega$, where $\Gamma_{\mathbf{n}}(\mathbf{x}, \mathbf{x}_\alpha)$ is the geodesic line generated by the function $\mathbf{n}(\mathbf{x})$. It is well known that $u_{\mathbf{n}}(\mathbf{x}, \mathbf{x}_\alpha)$ satisfies the eikonal equation [28, Chapter 3]

$$|\nabla_{\mathbf{x}} u_{\mathbf{n}}(\mathbf{x}, \mathbf{x}_\alpha)|^2 = \mathbf{a}(\mathbf{x}), \quad \mathbf{x} \in \Omega, \mathbf{x}_\alpha \in L_s. \tag{2.10}$$

Let $u_0(\mathbf{x}, \mathbf{x}_\alpha)$ be the travel time function in (2.8) corresponding to the background $\mathbf{a}_0$. Then

$$|\nabla_{\mathbf{x}} u_0(\mathbf{x}, \mathbf{x}_\alpha)|^2 = \mathbf{a}_0(\mathbf{x}), \quad \mathbf{x} \in \Omega, \mathbf{x}_\alpha \in L_s. \tag{2.11}$$

Due to (2.9) we represent $\nabla_{\mathbf{x}} u_{\mathbf{n}}(\mathbf{x}, \mathbf{x}_\alpha)$ as

$$\nabla_{\mathbf{x}} u_{\mathbf{n}}(\mathbf{x}, \mathbf{x}_\alpha) = \nabla_{\mathbf{x}} u_0(\mathbf{x}, \mathbf{x}_\alpha) + \epsilon \nabla_{\mathbf{x}} u^{(1)}(\mathbf{x}, \mathbf{x}_\alpha). \tag{2.12}$$

Hence, ignoring the term with ϵ^2, we obtain

$$|\nabla_{\mathbf{x}} u_{\mathbf{n}}(\mathbf{x}, \mathbf{x}_\alpha)|^2 \approx |\nabla_{\mathbf{x}} u_0(\mathbf{x}, \mathbf{x}_\alpha)|^2 + 2\epsilon \nabla_{\mathbf{x}} u_0(\mathbf{x}, \mathbf{x}_\alpha) \nabla_{\mathbf{x}} u^{(1)}(\mathbf{x}, \mathbf{x}_\alpha). \tag{2.13}$$

Denoting

$$u^{(1)} := u \tag{2.14}$$

and comparing (2.13) with (2.9) and (2.11), we obtain

$$\frac{\nabla_{\mathbf{x}} u_0(\mathbf{x}, \mathbf{x}_\alpha)}{\sqrt{\mathbf{a}_0(\mathbf{x})}} \cdot \nabla_{\mathbf{x}} u(\mathbf{x}, \mathbf{x}_\alpha) = p(\mathbf{x}). \tag{2.15}$$

Thus, (2.15) is the "linearization" of the nonlinear equation (2.10). By (2.11),

$$|\nabla_{\mathbf{x}} u_0(\mathbf{x}, \mathbf{x}_\alpha)| / \sqrt{\mathbf{a}_0(\mathbf{x})} \equiv 1.$$

Hence, this is a unit vector, which is tangent to the curve $\Gamma_0(\mathbf{x}, \mathbf{x}_\alpha)$ at the point $\mathbf{x}$ [28, Chapter 3]. Hence, the left-hand side of (2.15) is the derivative of the function $u(\mathbf{x}, \mathbf{x}_\alpha)$ along the curve $\Gamma_0(\mathbf{x}, \mathbf{x}_\alpha)$. Thus, integrating, we obtain [28, Chapter 3]

$$u(\mathbf{x}, \mathbf{x}_\alpha) = \int_{\Gamma_0(\mathbf{x}, \mathbf{x}_\alpha)} p(\boldsymbol{\xi}) d\sigma(\boldsymbol{\xi}). \tag{2.16}$$

Let $\partial\Omega_{\text{sm}}$ be the smooth part of the boundary $\partial\Omega$ of the domain Ω. For each $\alpha \in (-\overline{\alpha}, \overline{\alpha})$, define

$$\partial\Omega_\alpha^- = \{\mathbf{x} \in \partial\Omega_{\text{sm}} : \nabla_{\mathbf{x}} u_0(\mathbf{x}, \mathbf{x}_\alpha) \cdot \nu(\mathbf{x}) < 0\},$$
$$\partial\Omega_\alpha^+ = \{\mathbf{x} \in \partial\Omega_{\text{sm}} : \nabla_{\mathbf{x}} u_0(\mathbf{x}, \mathbf{x}_\alpha) \cdot \nu(\mathbf{x}) > 0\},$$

where $\mathbf{x}_\alpha = (\alpha, 0, \dots, 0) \in L_{\text{s}}$ and $\nu(\mathbf{x})$ is the outward-looking unit normal vector at the point $\mathbf{x} \in \partial\Omega_{\text{sm}}$. If $\mathbf{n}_0 \equiv 1$, then $\Gamma_0(\mathbf{x}_1, \mathbf{x}_2)$ is the line segment connecting these two points. Hence, it follows from (2.1), (2.6), (2.7), (2.12), and (2.14) that

$$u(\mathbf{x}, \mathbf{x}_\alpha) = 0, \mathbf{x} \in \partial\Omega_\alpha^-. \tag{2.17}$$

The aim of this paper is to solve the following inverse problem.

Problem 2.1 (linearized travel time tomography problem). Let the function $u = u(\mathbf{x}, \mathbf{x}_\alpha) \in C^1\left(\overline{\Omega} \times [-\overline{\alpha}, \overline{\alpha}]\right)$ be the solution of boundary value problem (2.15), (2.17). Given the data $f(\mathbf{x}, \mathbf{x}_\alpha)$,

$$f(\mathbf{x}, \mathbf{x}_\alpha) = \begin{cases} u(\mathbf{x}, \mathbf{x}_\alpha), \ \mathbf{x} \in \partial\Omega_\alpha^+, \mathbf{x}_\alpha \in L_{\text{s}}, \\ 0, \ \mathbf{x} \in \partial\Omega_\alpha^-, \mathbf{x}_\alpha \in L_{\text{s}}, \end{cases} \tag{2.18}$$

determine the function $p(\mathbf{x})$, $\mathbf{x} \in \Omega$.

Note that the data (2.18) are nonredundant ones. Indeed, the source $\mathbf{x}_\alpha \in L_{\text{s}}$ depends on one variable, and the point $\mathbf{x} \in \partial\Omega_\alpha^+$ depends on $d-1$ variables. Hence, the function $f(\mathbf{x}, \mathbf{x}_\alpha)$ depends on d variables, so does the target unknown function $p(\mathbf{x})$.

From now on, to separate the coordinate number d of the point $\mathbf{x}$, we write $\mathbf{x} = (x_1, \dots, x_{d-1}, z)$. The transport equation in (2.15) reads as

$$\frac{\partial_z u_0(\mathbf{x}, \mathbf{x}_\alpha)}{\sqrt{\mathbf{a}_0(\mathbf{x})}} \partial_z u(\mathbf{x}, \mathbf{x}_\alpha) + \sum_{i=1}^{d-1} \frac{\partial_{x_i} u_0(\mathbf{x}, \mathbf{x}_\alpha)}{\sqrt{\mathbf{a}_0(\mathbf{x})}} \partial_{x_i} u(\mathbf{x}, \mathbf{x}_\alpha) = p(\mathbf{x}), \tag{2.19}$$

which is equivalent to

$$\partial_z u_0(\mathbf{x}, \mathbf{x}_\alpha) \partial_z u(\mathbf{x}, \mathbf{x}_\alpha) + \sum_{i=1}^{d-1} \partial_{x_i} u_0(\mathbf{x}, \mathbf{x}_\alpha) \partial_{x_i} u(\mathbf{x}, \mathbf{x}_\alpha) = \sqrt{\mathbf{a}_0(\mathbf{x})} p(\mathbf{x}) \tag{2.20}$$

for all $\mathbf{x} \in \Omega$, $\mathbf{x}_\alpha \in L_{\text{s}}$.

3. A boundary value problem for a system of coupled PDEs of the first order. This section aims to derive a system of PDEs, which can be stably solved by the quasi-reversibility method in the semifinite difference scheme. The solution of this

system yields the desired numerical solution to Problem 2.1. Recall that Problem 2.1 is the linearized travel time tomography problem, and it is labeled this way by its title.

We will employ a special basis of $L^2(-\overline{\alpha},\overline{\alpha})$, where $2\overline{\alpha}$ is the length of the line of source L_{sc}; see (2.6). For each $n = 1, 2, \ldots$, let $\phi_n(\alpha) = \alpha^{n-1}\exp(\alpha)$. The set $\{\phi_n\}_{n=1}^{\infty}$ is complete in $L^2(-\overline{\alpha},\overline{\alpha})$. Applying the Gram–Schmidt orthonormalization process to this set, we obtain a basis of $L^2(-\overline{\alpha},\overline{\alpha})$ named $\{\Psi_n\}_{n=1}^{\infty}$. We have the following proposition.

PROPOSITION 3.1 (see [11]). *The basis $\{\Psi_n\}_{n=1}^{\infty}$ satisfies the following properties:*

1. *Ψ_n is not identically zero for all $n \geq 1$.*
2. *For all $m, n \geq 1$,*

$$s_{mn} = \int_{-\overline{\alpha}}^{\overline{\alpha}} \Psi_n'(\alpha)\Psi_m(\alpha)d\alpha = \begin{cases} 1 & \text{if } m = n, \\ 0 & \text{if } n < m. \end{cases}$$

Thus, the matrix $S_N = (s_{mn})_{m,n=1}^{N}$ is invertible for all integers $N \geq 1$.

We now derive a system of PDEs for the Fourier coefficients of the function

$$w(\mathbf{x},\mathbf{x}_\alpha) = u(\mathbf{x},\mathbf{x}_\alpha)\partial_z u_0(\mathbf{x},\mathbf{x}_\alpha) \quad \mathbf{x}\in\Omega, \mathbf{x}_\alpha \in L_{\text{s}} \tag{3.1}$$

with respect to the basis $\{\Psi_n\}_{n=1}^{\infty}$. Differentiate (2.20) with respect to α. We obtain

$$\frac{\partial}{\partial\alpha}\Big[\partial_z u_0(\mathbf{x},\mathbf{x}_\alpha)\partial_z u(\mathbf{x},\mathbf{x}_\alpha) + \sum_{i=1}^{d-1}\partial_{x_i} u_0(\mathbf{x},\mathbf{x}_\alpha)\partial_{x_i} u(\mathbf{x},\mathbf{x}_\alpha)\Big] = 0 \tag{3.2}$$

for all $\mathbf{x}\in\Omega$, $\mathbf{x}_\alpha \in L_{\text{s}}$. From now on, we impose the following condition.

Assumption 3.1 (monotonicity condition in the z-direction). The traveling time function u_0, defined in (2.8) with $\mathbf{n}$ replaced by $\mathbf{n}_0$, is strictly increasing with respect to z. In other words, $\partial_z u_0(\mathbf{x},\mathbf{x}_\alpha) > 0$ for all $\mathbf{x} = (x_1,\ldots,x_{d-1},z) \in \Omega$ and for all $\mathbf{x}_\alpha \in L_{\text{s}}$.

Assumption 3.1 means that the higher in the z-direction, the longer the traveling time is. A sufficient condition for Assumption 3.1 to be true is formulated in (3.3) of Lemma 3.1. A similar monotonicity condition can be found in formulas (3.24) and (3.24′) of section 2 of Chapter 3 of [28]. Also, a similar condition was imposed in originating works for the 1D problem of Herglotz [5] and Wiechert and Zoeppritz [36]; see section 3 of Chapter 3 of [28]. Besides, Figures 5 and 10 of [35] justify this condition from the geophysical standpoint. Recall that by (2.5) and (2.2), $\mathbf{a}_0 \in C^2\left(\mathbb{R}^d\right)$ and $\mathbf{a}_0(\mathbf{x}) \geq 1$ in $\mathbb{R}^d$. Therefore, the following lemma follows immediately from Lemma 4.1 of [13].

LEMMA 3.1. *Let conditions* (2.2) *and* (2.5) *hold. Also, let*

$$\partial_z \mathbf{a}_0(\mathbf{x}) \geq 0 \text{ for all } \mathbf{x}\in\overline{\Omega}. \tag{3.3}$$

Then

$$\partial_z u_0(\mathbf{x},\mathbf{x}_\alpha) \geq \frac{a}{\sqrt{a^2+2}} \text{ for all } \mathbf{x}\in\overline{\Omega}, \alpha\in[-\overline{\alpha},\overline{\alpha}].$$

Although Lemma 3.1 is proven in [13] only in the 3D case, the proof in the $d-$D case is very similar and is, therefore, avoided. Let $w(\mathbf{x}, \mathbf{x}_\alpha)$ be the function defined in (3.1). Then

$$\partial_z u_0(\mathbf{x}, \mathbf{x}_\alpha)\partial_z u(\mathbf{x}, \mathbf{x}_\alpha) = \partial_z w(\mathbf{x}, \mathbf{x}_\alpha) - u(\mathbf{x}, \alpha)\partial_{zz} u_0(\mathbf{x}, \mathbf{x}_\alpha) = \partial_z w(\mathbf{x}, \mathbf{x}_\alpha) - w(\mathbf{x}, \alpha)\frac{\partial_{zz} u_0(\mathbf{x}, \mathbf{x}_\alpha)}{\partial_z u_0(\mathbf{x}, \mathbf{x}_\alpha)}. \tag{3.4}$$

Also, for $i = 1, \dots, d-1$,

$$\partial_{x_i} u(\mathbf{x}, \mathbf{x}_\alpha) = \frac{\partial}{\partial x_i}\left(\frac{w(\mathbf{x}, \mathbf{x}_\alpha)}{\partial_z u_0(\mathbf{x}, \mathbf{x}_\alpha)}\right) = \frac{\partial_{x_i} w(\mathbf{x}, \mathbf{x}_\alpha)\partial_z u_0(\mathbf{x}, \mathbf{x}_\alpha) - w(\mathbf{x}, \mathbf{x}_\alpha)\partial_{zx_i} u_0(\mathbf{x}, \mathbf{x}_\alpha)}{(\partial_z u_0(\mathbf{x}, \mathbf{x}_\alpha))^2} \tag{3.5}$$

for all $\mathbf{x} \in \Omega, \mathbf{x}_\alpha \in L_{\text{sc}}$. Combining (3.2), (3.4), and (3.5), we obtain

$$\frac{\partial}{\partial \alpha}\Big[\partial_z w(\mathbf{x}, \mathbf{x}_\alpha) - w(\mathbf{x}, \mathbf{x}_\alpha)\frac{\partial_{zz} u_0(\mathbf{x}, \mathbf{x}_\alpha)}{\partial_z u_0(\mathbf{x}, \mathbf{x}_\alpha)} + \sum_{i=1}^{d-1} \frac{\partial_{x_i} w(\mathbf{x}, \mathbf{x}_\alpha)\partial_z u_0(\mathbf{x}, \mathbf{x}_\alpha) - w(\mathbf{x}, \mathbf{x}_\alpha)\partial_{zx_i} u_0(\mathbf{x}, \mathbf{x}_\alpha)}{(\partial_z u_0(\mathbf{x}, \mathbf{x}_\alpha))^2}\partial_{x_i} u_0(\mathbf{x}, \mathbf{x}_\alpha)\Big] = 0. \tag{3.6}$$

This is equivalent to

$$\begin{aligned}\partial_{\alpha z} w(\mathbf{x}, \mathbf{x}_\alpha) &- \frac{\partial_{zz} u_0(\mathbf{x}, \mathbf{x}_\alpha)}{\partial_z u_0(\mathbf{x}, \mathbf{x}_\alpha)}\partial_\alpha w(\mathbf{x}, \mathbf{x}_\alpha) - \frac{\partial}{\partial \alpha}\left(\frac{\partial_{zz} u_0(\mathbf{x}, \mathbf{x}_\alpha)}{\partial_z u_0(\mathbf{x}, \mathbf{x}_\alpha)}\right) w(\mathbf{x}, \mathbf{x}_\alpha) \\ &+ \sum_{i=1}^{d-1}\Big[\frac{\partial_{x_i} u_0(\mathbf{x}, \mathbf{x}_\alpha)}{\partial_z u_0(\mathbf{x}, \mathbf{x}_\alpha)}\partial_{\alpha x_i} w(\mathbf{x}, \mathbf{x}_\alpha) + \frac{\partial}{\partial \alpha}\left(\frac{\partial_{x_i} u_0(\mathbf{x}, \mathbf{x}_\alpha)}{\partial_z u_0(\mathbf{x}, \mathbf{x}_\alpha)}\right)\partial_{x_i} w(\mathbf{x}, \mathbf{x}_\alpha) \\ &- \frac{\partial_{zx_i} u_0(\mathbf{x}, \mathbf{x}_\alpha)\partial_{x_i} u_0(\mathbf{x}, \mathbf{x}_\alpha)}{(\partial_z u_0(\mathbf{x}, \mathbf{x}_\alpha))^2}\partial_\alpha w(\mathbf{x}, \mathbf{x}_\alpha) \\ &- \frac{\partial}{\partial \alpha}\left(\frac{\partial_{zx_i} u_0(\mathbf{x}, \mathbf{x}_\alpha)\partial_{x_i} u_0(\mathbf{x}, \mathbf{x}_\alpha)}{(\partial_z u_0(\mathbf{x}, \mathbf{x}_\alpha))^2}\right) w(\mathbf{x}, \mathbf{x}_\alpha)\Big] = 0.\end{aligned} \tag{3.7}$$

We recall now the orthonormal basis $\{\Psi_n\}_{n=1}^\infty$ constructed at the beginning of this section. For each $\mathbf{x} \in \Omega$ and for all $\mathbf{x}_\alpha \in L_{\text{sc}}$, we write

$$w(\mathbf{x}, \mathbf{x}_\alpha) = \sum_{n=1}^\infty w_n(\mathbf{x})\Psi_n(\alpha) \approx \sum_{n=1}^N w_n(\mathbf{x})\Psi_n(\alpha), \tag{3.8}$$

$$w_n(\mathbf{x}) = \int_{-\overline{\alpha}}^{\overline{\alpha}} w(\mathbf{x}, \mathbf{x}_\alpha)\Psi_n(\alpha)d\alpha. \tag{3.9}$$

The "cutoff" number N is chosen numerically. We discuss the choice of N in more details in section 5. Following our approximate mathematical model introduced in section 1, we assume that the approximation $\approx$ in (3.8) is an equality as well as

$$\partial_\alpha w(\mathbf{x}, \mathbf{x}_\alpha) = \sum_{n=1}^N w_n(\mathbf{x})\Psi_n'(\alpha). \tag{3.10}$$

Plugging (3.8) and (3.10) into (3.7) gives

$$\sum_{n=1}^{N}\partial_z w_n(\mathbf{x})\Psi_n'(\alpha)-\frac{\partial_{zz}u_0(\mathbf{x},\mathbf{x}_\alpha)}{\partial_z u_0(\mathbf{x},\mathbf{x}_\alpha)}\sum_{n=1}^{N}w_n(\mathbf{x})\Psi_n'(\alpha)$$
$$-\frac{\partial}{\partial\alpha}\left(\frac{\partial_{zz}u_0(\mathbf{x},\mathbf{x}_\alpha)}{\partial_z u_0(\mathbf{x},\mathbf{x}_\alpha)}\right)\sum_{n=1}^{N}w_n(\mathbf{x})\Psi_n(\alpha)+\sum_{i=1}^{d-1}\Big[\frac{\partial_{x_i}u_0(\mathbf{x},\mathbf{x}_\alpha)}{\partial_z u_0(\mathbf{x},\mathbf{x}_\alpha)}\sum_{n=1}^{N}\partial_{x_i}w_n(\mathbf{x})\Psi_n'(\alpha)$$
$$+\frac{\partial}{\partial\alpha}\left(\frac{\partial_{x_i}u_0(\mathbf{x},\mathbf{x}_\alpha)}{\partial_z u_0(\mathbf{x},\mathbf{x}_\alpha)}\right)\sum_{n=1}^{N}\partial_{x_i}w_n(\mathbf{x})\Psi_n(\alpha)-\frac{\partial_{zx_i}u_0(\mathbf{x},\mathbf{x}_\alpha)\partial_{x_i}u_0(\mathbf{x},\mathbf{x}_\alpha)}{(\partial_z u_0(\mathbf{x},\mathbf{x}_\alpha))^2}\sum_{n=1}^{N}w_n(\mathbf{x})\Psi_n'(\alpha)$$
$$-\frac{\partial}{\partial\alpha}\left(\frac{\partial_{zx_i}u_0(\mathbf{x},\mathbf{x}_\alpha)\partial_{x_i}u_0(\mathbf{x},\mathbf{x}_\alpha)}{(\partial_z u_0(\mathbf{x},\mathbf{x}_\alpha))^2}\right)\sum_{n=1}^{N}w_n(\mathbf{x})\Psi_n(\alpha)\Big]=0.$$

For each $m\in\{1,\dots,N\}$, multiply the latter equation by $\Psi_m(\alpha)$, and then integrate the resulting equation with respect to α. We get

$$\sum_{n=1}^{N}s_{mn}\partial_z w_n(\mathbf{x})+\sum_{n=1}^{N}a_{mn}(\mathbf{x})w_n(\mathbf{x})+\sum_{n=1}^{N}\sum_{i=1}^{d-1}b_{mn,i}(\mathbf{x})\partial_{x_i}w_n(\mathbf{x})=0 \tag{3.11}$$

for all $\mathbf{x}\in\Omega$, where s_{mn} is defined as in Proposition 3.1,

$$a_{mn}(\mathbf{x})=\int_{-\overline{\alpha}}^{\overline{\alpha}}\Bigg[-\frac{\partial_{zz}u_0(\mathbf{x},\mathbf{x}_\alpha)}{\partial_z u_0(\mathbf{x},\mathbf{x}_\alpha)}\Psi_n'(\alpha)-\frac{\partial}{\partial\alpha}\left(\frac{\partial_{zz}u_0(\mathbf{x},\mathbf{x}_\alpha)}{\partial_z u_0(\mathbf{x},\mathbf{x}_\alpha)}\right)\Psi_n(\alpha)$$
$$-\sum_{i=1}^{d-1}\frac{\partial}{\partial\alpha}\left(\frac{\partial_{zx_i}u_0(\mathbf{x},\mathbf{x}_\alpha)\partial_{x_i}u_0(\mathbf{x},\mathbf{x}_\alpha)}{(\partial_z u_0(\mathbf{x},\mathbf{x}_\alpha))^2}\right)\Psi_n'(\alpha)$$
$$-\sum_{i=1}^{d-1}\frac{\partial}{\partial\alpha}\left(\frac{\partial_{zx_i}u_0(\mathbf{x},\mathbf{x}_\alpha)\partial_{x_i}u_0(\mathbf{x},\mathbf{x}_\alpha)}{(\partial_z u_0(\mathbf{x},\mathbf{x}_\alpha))^2}\right)\Psi_n(\alpha)\Bigg]\Psi_m(\alpha)d\alpha, \tag{3.12}$$

and for $i=1,\dots,d-1$,

$$b_{mn,i}(\mathbf{x})=\int_{-\overline{\alpha}}^{\overline{\alpha}}\Big[\frac{\partial_{x_i}u_0(\mathbf{x},\mathbf{x}_\alpha)}{\partial_z u_0(\mathbf{x},\mathbf{x}_\alpha)}\Psi_n'(\alpha)+\frac{\partial}{\partial\alpha}\left(\frac{\partial_{x_i}u_0(\mathbf{x},\mathbf{x}_\alpha)}{\partial_z u_0(\mathbf{x},\mathbf{x}_\alpha)}\right)\Psi_n(\alpha)\Big]\Psi_m(\alpha)d\alpha \tag{3.13}$$

for all $\mathbf{x}\in\Omega$. For each $\mathbf{x}\in\Omega$, let $W(\mathbf{x})=(w_1(\mathbf{x}),\dots,w_N(\mathbf{x}))^T$, $S=(s_{mn})_{m,n=1}^N$, $A(\mathbf{x})=(a_{mn}(\mathbf{x}))_{m,n=1}^N$, and $B_i(\mathbf{x})=(b_{mn,i}(\mathbf{x}))_{m,n=1}^N$ for $i=1,\dots,d-1$. Since (3.11) holds true for every $m=1,\dots,N$, it can be rewritten as

$$S_N\partial_z W(\mathbf{x})+A(\mathbf{x})W(\mathbf{x})+\sum_{i=1}^{d-1}B_i(\mathbf{x})\partial_{x_i}W(\mathbf{x})=0. \tag{3.14}$$

Since S is invertible (see Proposition 3.1), (3.14) implies the following system of transport equations:

$$\partial_z W(\mathbf{x})+S_N^{-1}A(\mathbf{x})W(\mathbf{x})+\sum_{i=1}^{d-1}S_N^{-1}B_i(\mathbf{x})\partial_{x_i}W(\mathbf{x})=0,\quad \mathbf{x}\in\Omega. \tag{3.15}$$

The boundary data for W are

$$W|_{\partial\Omega}=F(\mathbf{x})=(f_n)_{n=1}^N,\quad f_n(\mathbf{x})=\int_{-\overline{\alpha}}^{\overline{\alpha}}f(\mathbf{x},\mathbf{x}_\alpha)\partial_z u_0(\mathbf{x},\mathbf{x}_\alpha)\Psi_n(\alpha)d\alpha, \tag{3.16}$$

where f is the given data; see (2.18).

Remark 3.2 (the approximation context). Due to the truncation in (3.8), (3.15) is within the framework of our approximate mathematical model mentioned in the introduction. Since this paper is concerned with computational rather than theoretical results, this model is acceptable. Our approximation leads to good numerical results in section 5.

Remark 3.3. Problem 2.1 is reduced to the problem of finding the vector valued function W satisfying the system (3.15) and the boundary condition (3.16). Assume this vector function is computed, and denote it as $W^{\text{comp}} = (w_1^{\text{comp}}, \dots, w_n^{\text{comp}})$. Then we can compute the function $w^{\text{comp}}(\mathbf{x}, \mathbf{x}_\alpha)$ and then the function $u^{\text{comp}}(\mathbf{x}, \mathbf{x}_\alpha)$ sequentially via (3.8) and (3.1). The computed target function $p^{\text{comp}}(\mathbf{x})$ is given by (2.19).

We find an approximate solution of the boundary value problem (3.15)–(3.16) by the quasi-reversibility method. This means that we minimize the functional

$$J_\epsilon(W) = \int_\Omega \left|\partial_z W(\mathbf{x}) + \sum_{i=1}^{d-1} S_N^{-1} B_i(\mathbf{x}) \partial_{x_i} W(\mathbf{x}) + S_N^{-1} A(\mathbf{x}) W(\mathbf{x})\right|^2 d\mathbf{x} + \epsilon \|W\|^2_{H^1(\Omega)^N} \tag{3.17}$$

on the set of vector functions $W \in H^1(\Omega)^N$ satisfying the boundary constraint (3.16). Here, the space $H^1(\Omega)^N = \underbrace{H^1(\Omega) \times \cdots \times H^1(\Omega)}_{N}$ with the commonly defined norm. Similarly to [32], we analyze the functional $J_\epsilon(W)$ for the case when derivatives in (3.17) are written in finite differences.

4. The quasi-reversibility method in the finite differences. For brevity, we describe and analyze here the quasi-reversibility method in the case when $d = 2$. The arguments for higher dimensions can be done in the same manner. In 2D, $\Omega = (-R, R) \times (a, b)$. We arrange an $N_x \times N_z$ grid of points on $\overline{\Omega}$,

$$\mathcal{G} = \{(x_i, z_j) : x_i = -R + (i-1)h_x, z_j = a + (j-1)h_z, \quad i = 1, \dots, N_x, j = 1, \dots, N_z\}, \tag{4.1}$$

where $h_x \in [h_0, \beta_x)$ and $h_z \in (0, \beta_z)$ are grid step sizes in the x and z directions, respectively, and $h_0, \beta_x, \beta_z > 0$ are certain numbers. Here, N_x and N_z are two positive integers. Let $\mathbf{h} = (h_x, h_z)$. We define the discrete set $\Omega^{\mathbf{h}}$ as the set of those points of the set (4.1) which are interior points of the rectangle Ω and $\partial\Omega^{\mathbf{h}}$ is the set of those points of the set (4.1) which are located on the boundary of Ω:

$$\begin{aligned}
\Omega^{\mathbf{h}} &= \{(x_i, z_j) : x_i = -R + (i-1)h_x, z_j = a + (j-1)h_z : \\
&\qquad i = 2, \dots, N_x - 1; j = 2, \dots, N_z - 1\} \\
\partial\Omega^{\mathbf{h}} &= \{(\pm R, z_j) : j = 1, \dots, N_z\} \cup \{(x_i, z) : i = 1, \dots, N_x, z \in \{a, b\}\}, \\
\overline{\Omega}^{\mathbf{h}} &= \Omega^{\mathbf{h}} \cup \partial\Omega^{\mathbf{h}}.
\end{aligned}$$

For any continuous function v defined on Ω, its finite difference version is $v^{\mathbf{h}} = v|_{\mathcal{G}}$. Here, $\mathbf{h}$ denotes the pair (h_x, h_z). The partial derivatives of the function v are given via forward finite differences as

$$\begin{aligned}
\partial_x^{h_x} v^{\mathbf{h}}(x_i, z_j) &= \frac{v^{\mathbf{h}}(x_{i+1}, z_j) - v^{\mathbf{h}}(x_i, z_j)}{h_x}, \\
\partial_z^{h_z} v^{\mathbf{h}}(x_i, z_j) &= \frac{v(x_i, z_{j+1}) - v(x_i, z_j)}{h_z}
\end{aligned} \tag{4.2}$$

for $i = 0, \dots, N_x - 1$ and $j = 0, \dots, N_z - 1$. We denote the finite difference analogues of the spaces $L^2(\Omega)$ and $H^1(\Omega)$ as $L^{2,\mathbf{h}}(\Omega)$ and $H^{1,\mathbf{h}}(\Omega)$. Norms in these spaces are defined as

$$\|v^{\mathbf{h}}\|_{L^{2,\mathbf{h}}(\Omega^{\mathbf{h}})} = \left[h_x h_z \sum_{i=0}^{N_x} \sum_{j=0}^{N_z} \left[v^{\mathbf{h}}(x_i, z_j)\right]^2\right]^{1/2},$$

$$\|v^{\mathbf{h}}\|_{H^{1,\mathbf{h}}(\Omega^{\mathbf{h}})} = \Big[\|v^{\mathbf{h}}\|^2_{L^{2,\mathbf{h}}(\Omega^{\mathbf{h}})} + h_x h_z \sum_{i=0}^{N_x-1} \sum_{j=0}^{N_z-1} \left[\partial_x^{h_x} v^{\mathbf{h}}(x_i, z_j)\right]^2 + \left[\partial_z^{h_z} v^{\mathbf{h}}(x_i, z_j)\right]^2\Big]^{1/2}.$$

Let $F^{\mathbf{h}} = F\,|_{\partial\Omega^{\mathbf{h}}}$. The problem (3.15)–(3.16) becomes

$$L^h\left(W^{\mathbf{h}}\right) = \partial_z^{h_z} W^{\mathbf{h}}(x_i, z_j) + S_N^{-1} B_1(\mathbf{x}_i, z_j)\partial_x^{h_x} W^{\mathbf{h}}(x_i, z_j) + S_N^{-1} A(x_i, z_j) W^{\mathbf{h}}(x_i, z_j) = 0 \tag{4.3}$$

for $i = 0, \dots, N_x - 1; j = 0, \dots, N_z - 1$ and

$$W^{\mathbf{h}}\,|_{\partial\Omega^{\mathbf{h}}} = F^{\mathbf{h}}. \tag{4.4}$$

To solve problem (4.3)–(4.4) numerically, we introduce the finite difference version of the functional J_ϵ, defined in (3.17),

$$J_\epsilon^{\mathbf{h}}(W^{\mathbf{h}}) = h_x h_z \sum_{i=0}^{N_x-1} \sum_{j=0}^{N_z-1} \Big|\partial_z^{h_z} W^{\mathbf{h}}(x_i, z_j) + S_N^{-1} B_1(\mathbf{x}_i, z_j)\partial_x^{h_x} W^{\mathbf{h}}(z_i, z_j) + S_N^{-1} A(x_i, z_j) W^{\mathbf{h}}(x_i, z_j)\Big|^2 + \epsilon \|W^{\mathbf{h}}\|^2_{H_N^{1,\mathbf{h}}(\Omega^{\mathbf{h}})},$$

where $H_N^{1,\mathbf{h}}(\Omega^{\mathbf{h}}) = \left[H^{1,\mathbf{h}}(\Omega^{\mathbf{h}})\right]^N$ and similarly for $L_N^{2,\mathbf{h}}(\Omega^{\mathbf{h}})$. We consider the following problem.

Problem 4.1 (minimization problem). Minimize the functional $J_\epsilon^{\mathbf{h}}(W^{\mathbf{h}})$ on the set of such vector functions $W^{\mathbf{h}} \in H_N^{1,\mathbf{h}}(\Omega^{\mathbf{h}})$ that satisfy boundary condition (4.4).

The convergence theory for this problem is formulated in Theorems 4.1 and 4.2. Proofs of these theorems follow closely the arguments of [32, section 5] and are, therefore, not repeated in this paper. Theorem 4.1 guarantees the existence and uniqueness of the minimizer of $J_\epsilon^{\mathbf{h}}(W^{\mathbf{h}})$, and this result can be proven on the basis of the Riesz theorem. The next natural although a more difficult question is about the convergence of regularized solutions (i.e., minimizers) to the exact one when the level of the noise in the data tends to zero, i.e., Theorem 4.2. As it is often the case in the quasi-reversibility method (see, e.g., [10]), a close analogue of Theorem 4.2 is proven in [32, section 5] via applying a new discrete Carleman estimate: Recall that conventional Carleman estimates are in the continuous form. In other words, these two theorems confirm the effectiveness of our proposed numerical method for solving Problem 2.1.

THEOREM 4.1 (existence and uniqueness of the minimizer). *For any* $\mathbf{h} = (h_x, h_z)$ *with* $h_x \in [h_0, \beta_x), h_z \in (0, \beta_z)$, *any* $\epsilon > 0$, *and for any matrix* $F^{\mathbf{h}}$ *of boundary conditions, there exists unique minimizer* $W^{\mathbf{h}}_{\min,\epsilon} \in H_N^{1,\mathbf{h}}(\Omega^{\mathbf{h}})$ *of the functional satisfying boundary condition* (4.4).

As it is always the case in the regularization theory, assume now that there exists an "ideal" solution $W_*^{\mathbf{h}} \in H_N^{1,\mathbf{h}}(\Omega^{\mathbf{h}})$ of problem (4.3)–(4.4) satisfying the following boundary condition:

$$W_*^{\mathbf{h}} \mid_{\partial\Omega^{\mathbf{h}}} = F_*^{\mathbf{h}}, \tag{4.5}$$

where $F_*^{\mathbf{h}}$ is the "ideal" noiseless boundary data. Since $W_*^{\mathbf{h}}$ exists, (4.5) implies that there exists an extension $G_*^{\mathbf{h}} \in H_N^{1,\mathbf{h}}(\Omega^{\mathbf{h}})$ with $G_*^{\mathbf{h}} \mid_{\partial\Omega^{\mathbf{h}}} = F_*^{\mathbf{h}}$ of the matrix $F_*^{\mathbf{h}}$ in $\Omega^{\mathbf{h}}$. As to the data $F^{\mathbf{h}}$ in (4.4), we assume now that there exists an extension $G^{\mathbf{h}} \in H_N^{1,\mathbf{h}}(\Omega^{\mathbf{h}})$ with $G^{\mathbf{h}} \mid_{\partial\Omega^{\mathbf{h}}} = F^{\mathbf{h}}$ of $F^{\mathbf{h}}$ in $\Omega^{\mathbf{h}}$. Let $\delta > 0$ be the level of the noise in $G^{\mathbf{h}}$; see Remark 5.1. We assume that

$$\left\| G^{\mathbf{h}} - G_*^{\mathbf{h}} \right\|_{H_N^{1,\mathbf{h}}(\Omega^{\mathbf{h}})} < B\delta, \tag{4.6}$$

where the constant $B > 0$ is independent on δ.

It is convenient to replace the above notation of the minimizer $W_{\min,\epsilon}^{\mathbf{h}}$ with $W_{\min,\epsilon,\delta}^{\mathbf{h}}$, thus indicating its dependence on δ. In [32, section 5], to prove a direct analogue of Theorem 4.2 (formulated below), a new Carleman estimate for the finite difference operator $\partial_z^{h_z} v$ was proven first. The Carleman weight function of this estimate depends only on the discrete variable z. The value of this function at the point $z_j = a + (j-1)h_z$ is $e^{2\lambda(j-1)h_z}$, where $\lambda > 0$ is a parameter. This estimate is valid only if $\lambda h_z < 1$ (Lemma 4.7 of [32, section 5]). The latter explains the condition of Theorem 4.2 imposed on the grid step size h_z in the z-direction.

We now explain why we impose the condition that the grid step size h_x in the x-direction must be bounded from below as $h_x \geq h_0 = const. > 0$. Indeed, this bound guarantees that with a constant $C > 0$ independent on $\mathbf{h}$, we have $\left\| \partial_x^{h_x} W^{\mathbf{h}} \right\|_{L^{2,\mathbf{h}}(\Omega^{\mathbf{h}})} \leq C \left\| W^{\mathbf{h}} \right\|_{L^{2,\mathbf{h}}(\Omega^{\mathbf{h}})}$, which is exactly inequality (4.8) of [32, section 4]. Note that proofs of convergence results in [32, section 5] use the latter inequality quite essentially.

THEOREM 4.2 (convergence of regularized solutions). *Let conditions* (4.5) *and* (4.6) *be valid. Let* $L^{\mathbf{h}}$ *be the operator in* (4.3). *Let* $W_{\min,\epsilon,\delta}^{\mathbf{h}} \in H_N^{1,\mathbf{h}}(\Omega^{\mathbf{h}})$ *be the minimizer of the functional* $J_\epsilon^{\mathbf{h}}(W^{\mathbf{h}})$ *with boundary condition* (4.4). *Then there exists a sufficiently small number* $\overline{h}_z > 0$ *depending only on* h_0, a, b, R, N, $L^{\mathbf{h}}$ *such that the following estimate is valid for all* $(h_x, h_z) \in [h_0, \beta_x) \times \left(0, \overline{h}_z\right)$ *and all* $\epsilon, \delta > 0$ *with a constant* $C > 0$ *independent on* ϵ, δ*:*

$$\left\| W_{\min,\epsilon,\delta}^{\mathbf{h}} - W_*^{\mathbf{h}} \right\|_{L_N^{2,\mathbf{h}}(\Omega^{\mathbf{h}})} \leq C \left(\delta + \sqrt{\epsilon} \left\| W_*^{\mathbf{h}} \right\|_{H_N^{1,\mathbf{h}}(\Omega^{\mathbf{h}})} \right).$$

We also note that the Lipschitz stability estimate for problem (4.3)–(4.4) is valid as a direct analogue of Theorem 5.5 of [32, section 5]. Therefore, uniqueness also takes place for problem (4.3)–(4.4).

5. Numerical implementation. In this section, we solve Problem 2.1 in the 2D case. The domain Ω is

$$\Omega = (-1, 1) \times (1, 3). \tag{5.1}$$

The line of sources L_{s} is set to be $(-\overline{\alpha}, \overline{\alpha})$ with $\overline{\alpha} = 3$.

We solve the forward problem to compute the simulated data as follows. Given the background function $\mathbf{n}_0$, instead of solving the nonlinear eikonal equation (2.11), we find $u_0(\mathbf{x}, \mathbf{x}_\alpha)$ using (2.8). To do this, we first find the geodesic line $\Gamma_0(\mathbf{x}, \mathbf{x}_\alpha)$ in

(2.8) connecting points $\mathbf{x} \in \Omega$ and $\mathbf{x}_\alpha \in L_s$. We do the latter by using the 2D Fast Marching toolbox, which is built in MATLAB. The Fast Marching is very similar to the Dijkstra algorithm to find the shortest paths on graphs. We refer the reader to [31] for more details about Fast Marching. Next, with this geodesic line $\Gamma_0(\mathbf{x}, \mathbf{x}_\alpha)$ in hand, we compute the function $u(\mathbf{x}, \mathbf{x}_\alpha)$ via (2.16). It is clear that this function u solves (2.15). The point $\mathbf{x}_\alpha$ above is chosen as $(\alpha_i, 0)$, where $\alpha_i = 2(i-1)\overline{\alpha}/N_\alpha$. We set in our computations $N_\alpha = 209$.

Remark 5.1. Denote by $f^*(\mathbf{x}, \mathbf{x}_\alpha)$ the noiseless data $u(\mathbf{x}, \mathbf{x}_\alpha)$, $\mathbf{x} \in \partial\Omega$, $\mathbf{x}_\alpha \in L_s$. The corresponding noisy data at the noise level $\delta > 0$ are set as

$$f^\delta(\mathbf{x}, \mathbf{x}_\alpha) = f^*(\mathbf{x}, \mathbf{x}_\alpha)(1 + \delta \text{rand}(\mathbf{x}, \mathbf{x}_\alpha)), \ \mathbf{x} \in \partial\Omega_\alpha^+, \mathbf{x}_\alpha \in L_s, \tag{5.2}$$

where rand is the uniformly distributed function of random numbers taking values in the range $[-1, 1]$. Recall that by (2.18), $f^*(\mathbf{x}, \mathbf{x}_\alpha) = 0$ for $\mathbf{x} \in \partial\Omega_\alpha^-$. This noise generates a noise in the boundary condition $F^{\mathbf{h}}$ in (4.4). Hence, using (4.5), we obtain $F^{\mathbf{h}} = F_*^{\mathbf{h}} + \sigma^{\mathbf{h}}$, where $\sigma^{\mathbf{h}}$ is generated by the noisy part of (5.2).

The choice of appropriate values of parameters is always a difficult task. We have selected an appropriate cutoff number N in (3.8) by a trial-and-error procedure. More precisely, we took Test 4 in subsection 5.2 with the noise level 5% as a reference test and have selected such a value of N, which gave us the best reconstruction result. We have selected $N = 35$ this way. Then we have used the same $N = 35$ for all other tests.

5.1. Computing W^{comp}. We arrange the grid $\mathcal{G}$ in $\overline{\Omega}$ as in (4.1). For simplicity, we choose $N_{\mathbf{x}} = N_x = N_z$. The step size $h = h_x = h_z = 2R/(N_{\mathbf{x}} - 1)$. We observe numerically that the matrix S_N^{-1}, present in the definition of J_ϵ in (3.17), contains some large numbers. This causes some unwanted errors in computation. Therefore, using (3.14), we slightly modify the functional J_ϵ of (3.17) as

$$I_\epsilon(W) = \int_\Omega |S_N \partial_z W(\mathbf{x}) + A(\mathbf{x})W(\mathbf{x}) + \sum_{i=1}^{d-1} B_i(\mathbf{x})\partial_{x_i} W(\mathbf{x})|^2 d\mathbf{x} + \epsilon \|W\|^2_{H^1(\Omega)^N} + \epsilon \left(\|W_{xx}\|^2_{L^2(\Omega)^N} + \|W_{zz}\|^2_{L^2(\Omega)^N} \right). \tag{5.3}$$

We have numerically observed that the additional regularization term with the second derivatives in (5.3) is crucial. If this term is absent, then our numerical results do not meet our expectations; see Figure 1(g).

Remark 5.2. The above Theorems 4.1 and 4.2 are valid only for the case when the regularization term with the second derivatives is absent in (5.3). We also recall that proofs of those theorems are presented in [32, section 5]. We are not sure that those theorems can be extended to the case when the second derivatives are present in (5.3). Thus, we have a discrepancy between the theory and computations. It is well known, however, that such discrepancies quite often occur in numerical studies of truly hard problems, such as this publication.

The procedure of computing $p(\mathbf{x})$ is summarized in Algorithm 5.1.

In all tests with all noise levels in the data, we use $\epsilon = 10^{-8}$. This value was chosen by a trial-and-error procedure. The finite difference version of the functional

Algorithm 5.1 The procedure to solve Problem 2.1

1: Choose the cutoff number $N = 35$. Find $\{\Psi_n\}_{n=1}^N$.
2: Compute the boundary data of the vector valued function $W(\mathbf{x})$.
3: Minimize the functional $I_\epsilon(W)$ subjected to the boundary condition (3.16) to obtain $W^{\text{comp}}(\mathbf{x})$, $\mathbf{x} \in \Omega$.
4: Set $w^{\text{comp}}(\mathbf{x}, \mathbf{x}_\alpha) = \sum_{n=1}^N w_n^{\text{comp}} \Psi_n(\alpha)$, $\mathbf{x} \in \Omega$, $\alpha \in [-\overline{\alpha}, \overline{\alpha}]$.
5: Set $u^{\text{comp}} = w^{\text{comp}}/\partial_z u_0$. Compute p^{comp} by the average of the left-hand side of (2.20), namely,

$$p^{\text{comp}} = \frac{1}{2\overline{\alpha}\sqrt{\mathbf{a}_0(\mathbf{x})}} \int_{-\overline{\alpha}}^{\overline{\alpha}} \Big[\partial_z u_0(\mathbf{x}, \mathbf{x}_\alpha)\partial_z u^{\text{comp}}(\mathbf{x}, \mathbf{x}_\alpha) + \sum_{i=1}^{d-1} \partial_{x_i} u_0(\mathbf{x}, \mathbf{x}_\alpha)\partial_{x_i} u^{\text{comp}}(\mathbf{x}, \mathbf{x}_\alpha)\Big] d\alpha. \tag{5.4}$$

I_ϵ for $d = 2$ is

$$\begin{aligned} I_\epsilon^h(W) = h^2 \sum_{m=1}^N \sum_{i,j=1}^{N_{\mathbf{x}}-1} \Big| \sum_{n=1}^N \Big[& \frac{s_{mn}[w_n(x_i, z_{j+1}) - w_n(x_i, z_j)]}{h} \\ & + a_{mn}(x_i, z_j) w(x_i, y_j) + \frac{b_{mn}(x_i, z_j)(w(x_{i+1}, z_j) - w(x_i, z_j))}{h}\Big]\Big|^2 \\ + \epsilon h^2 \sum_{n=1}^N \sum_{i,j=0}^{N_{\mathbf{x}}} |w_n(x_i, z_j)|^2 + \epsilon h^2 & \sum_{n=1}^N \sum_{i,j=0}^{N_{\mathbf{x}}-1} \left[|\partial_x^h w_n(x_i, z_j)|^2 + |\partial_z^h w_n(x_i, z_j)|^2\right] \\ & + \epsilon h^2 \sum_{n=1}^N \sum_{i,j=1}^{N_{\mathbf{x}}-1} |\partial_{xx} w_n(x_i, z_j)|^2 + \epsilon h^2 \sum_{n=1}^N \sum_{i,j=1}^{N_{\mathbf{x}}-1} |\partial_{zz}^h w_n(x_i, z_j)|^2, \end{aligned}$$

where a_{mn} and $b_{mn} = b_{mn,1}$ in (3.12) and (3.13), respectively. The partial derivatives ∂_x^h and ∂_z^h are as in (4.2). The second derivatives in finite difference are understood as usual. We next line up the discrete vector valued function $w_n(x_i, z_j)$, $1 \le i, j \le N_{\mathbf{x}}$, $1 \le n \le N$ as the vector $(\mathfrak{w}_{\mathfrak{i}})_{\mathfrak{i}=1}^{N_{\mathbf{x}}^2 N}$ with

$$\mathfrak{w}_{\mathfrak{i}} = w_n(x_i, z_j), \tag{5.5}$$

where

$$\mathfrak{i} = (i-1)N_x N + (j-1)N + n. \tag{5.6}$$

The functional I_ϵ^h in the "lineup" version is

$$I_\epsilon^h(\mathfrak{w}) = h^2\Big[|\mathcal{L}\mathfrak{w}|^2 + \epsilon|D_x\mathfrak{w}|^2 + \epsilon|D_y\mathfrak{u}|^2 + \epsilon|L\mathfrak{w}|^2\Big]. \tag{5.7}$$

In (5.7),

1. $\mathcal{L}$ is the $N_{\mathbf{x}}^2 N \times N_{\mathbf{x}}^2 N$ matrix with entries given by
   (a) $(\mathcal{L})_{\mathfrak{ij}} = -s_{mn}/h + a_{mn}(x_i, z_j) - b_{mn}(x_i, y_j)/h$ for $\mathfrak{i} = (i-1)N_x N + (j-1)N + m$ and $\mathfrak{j} = (i-1)N_x N + (j-1)N + n$,

(b) $(\mathcal{L})_{\mathfrak{ij}} = b_{mn}(x_i, z_j)/h$ for $\mathfrak{i} = (i-1)N_xN + (j-1)N + m$ and $\mathfrak{j} = (i+1-1)N_xN + (j-1)N + n$,
(c) $(\mathcal{L})_{\mathfrak{ij}} = s_{mn}/h$ for $\mathfrak{i} = (i-1)N_xN + (j-1)N + m$ and $\mathfrak{j} = (i-1)N_xN + (j+1-1)N + n$,
(d) the other entries of $\mathcal{L}$ are 0
for $1 \le i, j \le N_{\mathbf{x}} - 1$ and $1 \le m, n \le N$;

2. D_x is the $N_{\mathbf{x}}^2 N \times N_{\mathbf{x}}^2 N$ matrix with entries given by
(a) $(D_x)_{\mathfrak{ii}} = -1/h$ for $\mathfrak{i} = (i-1)N_xN + (j-1)N + m$,
(b) $(D_x)_{\mathfrak{ij}} = 1/h$ for $\mathfrak{i} = (i-1)N_xN + (j-1)N + m$ and $\mathfrak{j} = (i+1-1)N_xN + (j-1)N + m$,
(c) the other entries of $\mathcal{L}$ are 0
for $1 \le i, j \le N_{\mathbf{x}} - 1$ and $1 \le m \le N$;

3. D_y is the $N_{\mathbf{x}}^2 N \times N_{\mathbf{x}}^2 N$ matrix with entries given by
(a) $(D_y)_{\mathfrak{ii}} = -1/h$ for $\mathfrak{i} = (i-1)N_xN + (j-1)N + m$,
(b) $(D_y)_{\mathfrak{ij}} = 1/h$ for $\mathfrak{i} = (i-1)N_xN + (j-1)N + m$ and $\mathfrak{j} = (i-1)N_xN + (j+1-1)N + m$,
(c) the other entries of $\mathcal{L}$ are 0
for $1 \le i, j \le N_{\mathbf{x}} - 1$ and $1 \le m \le N$;

4. L is the $N_{\mathbf{x}}^2 N \times N_{\mathbf{x}}^2 N$ matrix with entries given by
(a) $(L)_{\mathfrak{ii}} = -4/h^2$ for $\mathfrak{i} = (i-1)N_xN + (j-1)N + m$,
(b) $(L)_{\mathfrak{ij}} = -1/h^2$ for $\mathfrak{i} = (i-1)N_xN + (j-1)N + m$ and $\mathfrak{j} = (i \pm 1 - 1)N_xN + (j-1)N + m$,
(c) $(L)_{\mathfrak{ij}} = -1/h^2$ for $\mathfrak{i} = (i-1)N_xN + (j-1)N + m$ and $\mathfrak{j} = (i-1)N_xN + (j \pm 1 - 1)N + m$,
(d) the other entries of $\mathcal{L}$ are 0
for $2 \le i, j \le N_{\mathbf{x}} - 1$ and $1 \le m \le N$.

The minimizer $\mathfrak{w}$ of I_ϵ^h satisfies the equation

$$\mathcal{L}^T\mathcal{L} + \epsilon(\mathrm{Id} + D_x^T D_x + D_y^T D_y + L^T L)\mathfrak{w} = 0. \tag{5.8}$$

On the other hand, due to the constraint (3.16),

$$\mathcal{D}\mathfrak{w} = \mathfrak{f}, \tag{5.9}$$

where $\mathcal{D}$ is a $N_{\mathbf{x}}^2 N \times N_{\mathbf{x}}^2 N$ matrix and $\mathfrak{f}$ is a $N_{\mathbf{x}}^2 N$-dimensional vector, both of which are defined below:

1. $(\mathcal{D})_{\mathfrak{ii}} = 1$ for $\mathfrak{i} = (i-1)N_xN + (j-1)N + m$;
2. $(\mathfrak{f})_{\mathfrak{i}} = f_m(x_i, y_j)$ for $\mathfrak{i} = (i-1)N_xN + (j-1)N + m$;
3. the other entries of $\mathcal{L}$ and $\mathfrak{f}$ are 0

for $i \in \{1, N_{\mathbf{x}}\}$, $1 \le j \le N_{\mathbf{x}}$ or $2 \le i \le N_{\mathbf{x}} - 1$, $j \in \{1, N_{\mathbf{x}}\}$ and $1 \le m \le N$. Here, $(f_m)_{m=1}^N$ is in (3.16). Since the data might be noisy, we slightly modify the system constituted by (5.8) and (5.9) to a more stable version:

$$\left(\begin{bmatrix} \mathcal{L} \\ \mathcal{D} \end{bmatrix}^T \begin{bmatrix} \mathcal{L} \\ \mathcal{D} \end{bmatrix} + \epsilon(\mathrm{Id} + D_x^T D_x + D_y^T D_y + L^T L) \right) \mathfrak{w} = \begin{bmatrix} 0 \\ \mathfrak{f} \end{bmatrix}. \tag{5.10}$$

Solving the system (5.10), we obtain $\mathfrak{w}^{\mathrm{comp}}$. The values of components of vector valued function $W^{\mathrm{comp}}(\mathbf{x})$ at grid points are computed as $w_n(x_i, z_j) = \mathfrak{w}_{\mathfrak{i}}$ for $\mathfrak{i} = (i-1)N_xN + (j-1)N + m$, $1 \le i, j \le N_{\mathbf{x}}$, $1 \le m \le N$; see (5.5).

We have presented the implementation of step 3 in Algorithm 5.1. The other steps are straightforward.

Remark 5.3. In step 5 of Algorithm 5.1, when computing p^{comp} using (5.4), which involves ∇u^{comp}, we smooth out u^{comp} by replacing the value of $u^{\text{comp}}(x, y, \alpha)$, $\alpha \in [-\overline{\alpha}, \overline{\alpha}]$ by the average of u^{comp} on the rectangle of 5×5 points around the point (x, y). We also apply the same smoothing technique to the function p^{comp}.

5.2. Numerical tests. We perform four numerical tests in this paper. When indicating dependence of any function below on x, z, we assume that $(x, z) \in \Omega$, where the domain Ω is defined in (5.1). In all our tests, the noise level δ is as in (5.2).

Remark 5.4. In all our tests below, the function a_0 is far away from the constant background function. Therefore, Problem 2.1 is not considered as a small perturbation of the problem of the inverse Radon transform with incomplete data; see [16]. Some functions a_0 in our tests might not be smooth in $\mathbb{R}^2$. Still, $a_0 \in C^1(\overline{\Omega})$ in Tests 2 and 3. Thus, the second derivatives of the corresponding function u_0 are well defined in these two tests. Even though $a_0 \notin C^1(\overline{\Omega})$ in Test 1, numerically we have not experienced problems with second derivatives of the function u_0.

Test 1. The true source function p is given by

$$p^{\text{true}}(x, z) = \begin{cases} 8 & (x - 0.5)^2 + (z - 2)^2 < 0.24^2, \\ 5 & (x + 0.5)^2 + (z - 2)^2 < 0.22^2, \\ 0 & \text{otherwise.} \end{cases}$$

The background function $\mathbf{a}_0$ is

$$\mathbf{a}_0(x, z) = \begin{cases} 1 + 0.3(1 - x^2)(z^2 - 2) & \text{if } z^2 - 2 > 0, \\ 1 & \text{otherwise.} \end{cases}$$

The numerical results of this test are displayed in Figure 1.

The support of p^{true} in Test 1 consists of two discs. The value of the function p in the right disc is higher than the value in the left disc. Our method detects both these inclusions very well; see Figure 1(c)–1(f). There are some unwanted artifacts near $\partial\Omega$ where we measure the noisy data. The higher the level of noisy data, the more artifacts present. When the noise level $\delta = 5\%$, the computed maximal value of p^{comp} in the left inclusion is 4.97 (relative error 0.6%), and the computed maximal value of p^{comp} in the right inclusion is 7.79 (relative error 2.62%). When the noise level $\delta = 170\%$, the computed maximal value of p^{comp} in the left inclusion is 4.327 (relative error 13.46%), and the computed maximal value of p^{comp} in the right inclusion is 7.811 (relative error 2.36%).

To verify the necessity of the presence of the second derivatives in the regularization term of (5.3), we also conduct computations for Test 1 in the case when only the first derivatives are present in the regularization term of (5.3). The result for the case of 5% noise in the data is depicted in Figure 1(g). Comparison with Figure 1(c) makes it evident that the presence of the second derivatives in the regularization term of (5.3) is important.

Test 2. We test a complicated case when the support of p_{true} looks like a ring. In this test,

$$p^{\text{true}}(x, z) = \begin{cases} 2 & 0.55^2 < r^2 = x^2 + (z - 2)^2 < 0.75^2, \\ 0 & \text{otherwise.} \end{cases}$$

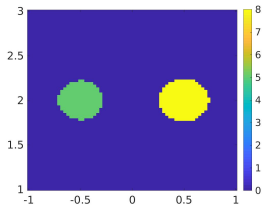

(a) The function p^{true}

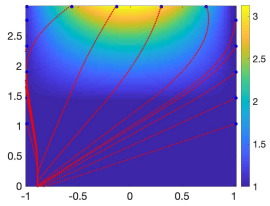

(b) The function $\mathbf{a}_0$ and some geodesic lines, generated by the Fast Marching package in MATLAB

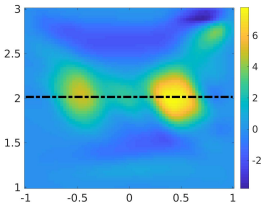

(c) The function p^{comp} computed by Algorithm 5.1 with 5% noise in the data

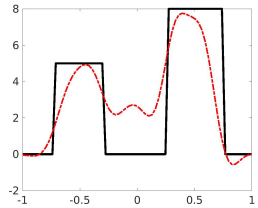

(d) The function p^{true} and p^{comp} with 5% noise in the data on the set $\{z = 2\}$, indicated by a dash-dot line in (c)

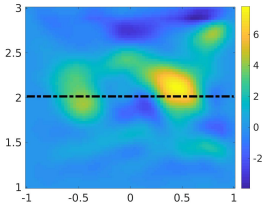

(e) The function p^{comp} computed by Algorithm 5.1 with 170% noise in the data

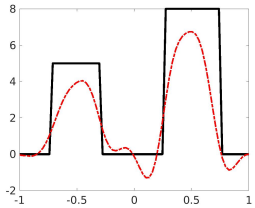

(f) The function p^{true} and p^{comp} with 170% noise in the data on the set $\{z = 2\}$, indicated by a dash-dot line in (e)

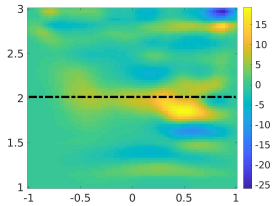

(g) The function p^{comp} in the case when second derivatives are absent in the regularization term of (5.3); 5% noise in the data; the image quality is significantly deteriorated compared with (c)

FIG. 1. *Test* 1. *The true and reconstructed source functions using Algorithm* 5.1 *from noisy data.*

The background function $\mathbf{a}_0$ is given by

$$\mathbf{a}_0(x,z) = \begin{cases} 1 + 0.25(x-0.5)^2 \ln(z) & z > 1, \\ 1 & \text{otherwise.} \end{cases}$$

The numerical results of this test are displayed in Figure 2.

In this test, it is evident that the reconstructed "ring" is acceptable; see Figure 2(c) and 2(e). The position of the ring is detected quite well; see Figures 2(d) and 2(f). When the noise level is 5%, the reconstructed maximal value of p^{comp} in the ring is 2.078 (relative error 3.9%). When the noise level is 100%, the reconstructed maximal value of p^{comp} in the ring is 2.329 (relative error 16.45%).

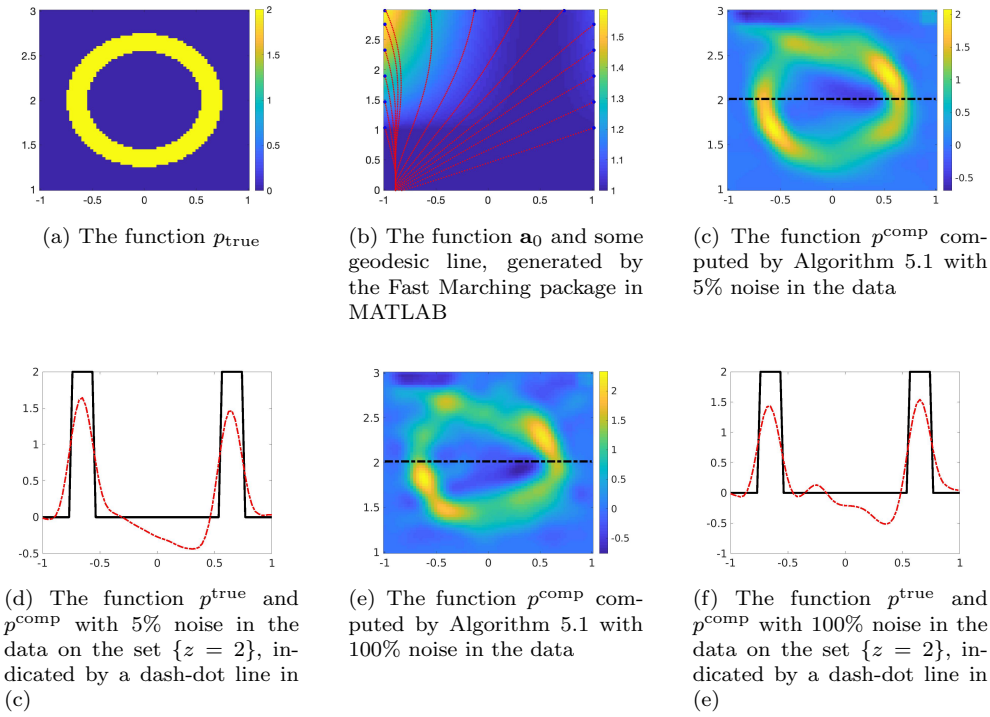

(a) The function p_{true}

(b) The function $\mathbf{a}_0$ and some geodesic line, generated by the Fast Marching package in MATLAB

(c) The function p^{comp} computed by Algorithm 5.1 with 5% noise in the data

(d) The function p^{true} and p^{comp} with 5% noise in the data on the set $\{z = 2\}$, indicated by a dash-dot line in (c)

(e) The function p^{comp} computed by Algorithm 5.1 with 100% noise in the data

(f) The function p^{true} and p^{comp} with 100% noise in the data on the set $\{z = 2\}$, indicated by a dash-dot line in (e)

FIG. 2. *Test* 2. *The true and reconstructed source functions using Algorithm* 5.1 *from noisy data.*

Test 3. We test an interesting and complicated case of the upside-down letter Y having both positive and negative values. In this test, the function p_{true} is given by

$$p^{\text{true}}(x,z) = \begin{cases} 2.5 & |x-(z-2)| < 0.35, \max\{|x|,|z-2|\} < 0.7, z < 2, x < 0, \\ -2.5 & |x+(z-2)| < 0.2, \max\{|x|,|z-2|\} < 0.7, z < 2, x > 0, \\ 2.5 & |x| < 0.2, \max\{|x|,|z-2|\} < 0.8, z > 2, x < 0, \\ -2.5 & |x| < 0.2, \max\{|x|,|z-2|\} < 0.8, z > 2, x > 0. \end{cases}$$

The background function $\mathbf{a}_0$ is given by

$$\mathbf{a}_0(x,z) = \begin{cases} 1 + 0.5(x+0.5)^2 \ln(z) & z > 1, \\ 1 & \text{otherwise.} \end{cases}$$

The numerical results of this test are displayed in Figure 3.

It is clear from Figure 3 that both positive and negative parts of the function $p(x,z)$ are successfully identified. When the noise level $\delta = 5\%$, the reconstructed maximal value of the positive part of p^{comp} is 2.186 (relative error 12.56%), and the reconstructed minimal value of p^{comp} of the negative part is -2.482 (relative error 0.72%.) When the noise level is $\delta = 100\%$, the reconstructed maximal value of p^{comp} of the positive part is 2.492 (relative error 0.32%), and the reconstructed minimal value of p^{comp} of the negative part is -3.327 (relative error 33.08%).

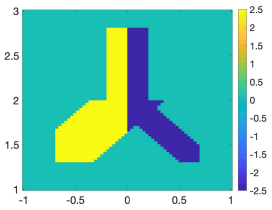

(a) The function p^{true}

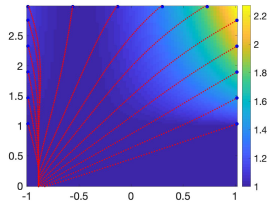

(b) The function $\mathbf{a}_0$ and some geodesic line, generated by the Fast Marching package in MATLAB

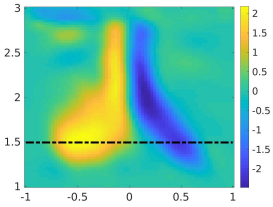

(c) The function p^{comp} computed by Algorithm 5.1 with 5% noise in the data

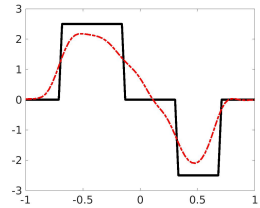

(d) The function p^{true} and p^{comp} with 5% noise in the data on the set $\{z = 1.5\}$, indicated by a dash-dot line in (c)

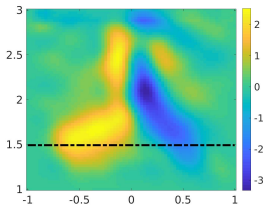

(e) The function p^{comp} computed by Algorithm 5.1 with 100% noise in the data

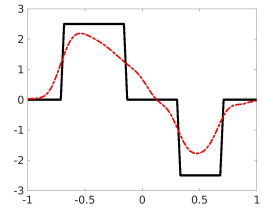

(f) The function p_{true} and p^{comp} with 100% noise in the data on the set $\{z = 1.5\}$, indicated by a dash-dot line in (e)

FIG. 3. *Test* 3. *The true and reconstructed source functions using Algorithm* 5.1 *from noisy data.*

Test 4. In this test, we reconstruct the letter λ. The function p^{true} is given by

$$p^{\text{true}}(x,z) = \begin{cases} 2 & |x-(z-2)| < 0.325, \max\{|x|,|z-2|\} < 0.7 \text{ and } x < -0.03, \\ 2 & |x+(z-2)| < 0.2 \text{ and } \max\{|x|,|z-2|\} < 0.7, \\ 0 & \text{otherwise.} \end{cases}$$

In this test, we choose $\mathbf{a}_0$ as

$$\mathbf{a}_0(x,z) = \begin{cases} 1 + x^2 \ln(z) & z > 1, \\ 1 & \text{otherwise.} \end{cases}$$

The numerical results of this test are displayed in Figure 4.

The letter λ and the values of the function p^{true} are successfully reconstructed. The computed position of λ is a quite accurate one; see Figure 4(d) and 4(f). When the noise level $\delta = 5\%$, the computed maximal value of p^{comp} is 2.24 (relative error 12.0%). When the noise level $\delta = 80\%$, the computed maximal value of p^{comp} is 2.375 (relative error 18.75%).

6. Concluding remarks. In this paper, we have developed a convergent numerical method of the solution of the linearized TTTP with nonredundant incomplete data. A good accuracy of numerical results with 5% noise in the data is demonstrated for rather complicated functions to be imaged. It is quite surprising that an acceptable accuracy of computational results is observed even for very a high level of noise in the data varying between 80% and 170%.

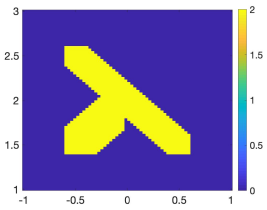

(a) The function p^{true}

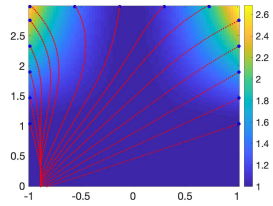

(b) The function $\mathbf{a}_0$ and some geodesic line, generated by the Fast Marching package in MATLAB

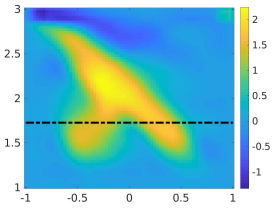

(c) The function p^{comp} by Algorithm 5.1 with 5% noise in the data

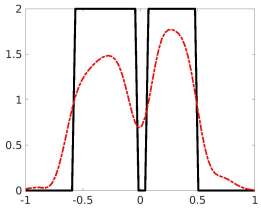

(d) The function p^{true} and p^{comp} with 5% noise in the data on the set $\{z = 1.7\}$, indicated by a dash-dot line in (c)

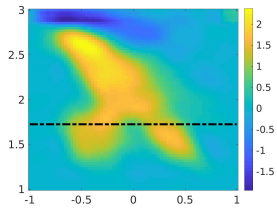

(e) The function p^{comp} computed by Algorithm 5.1 with 80% noise in the data

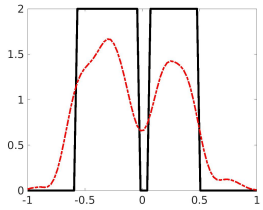

(f) The function p_{true} and p^{comp} with 80% noise in the data on the set $\{z = 1.7\}$, indicated by a dash-dot line in (e)

FIG. 4. *Test* 4. *The true and reconstructed source functions using Algorithm* 5.1 *from noisy data.*

REFERENCES

[1] I. N. BERNSTEIN AND M. L. GERVER, *On a problem of integral geometry for family of geodesics and the inverse kinematic problem of seismic*, Dokl. Akad. Nauk SSSR, 243 (1978).

[2] L. BOURGEOIS AND J. DARDÉ, *A duality-based method of quasi-reversibility to solve the Cauchy problem in the presence of noisy data*, Inverse Problems, 26 (2010), 095016.

[3] L. BOURGEOIS, D. PONOMAREV, AND J. DARDÉ, *An inverse obstacle problem for the wave equation in a finite time domain*, Inverse Probl. Imaging, 13 (2019), pp. 377–400.

[4] J. GUILLEMENT AND R. G. NOVIKOV, *Inversion of weighted Radon transforms via finite Fourier series weight approximation*, Inverse Probl. Sci. Eng., 22 (2013), pp. 787–802.

[5] G. HERGLOTZ, *Aœber die Elastizitaet der Erde bei Beruecksichtigung ihrer variablen Dichte*, Z. Math. Phys., 52 (1905), pp. 275–299.

[6] V. ISAKOV, *Inverse Problems for Partial Differential Equations*, 3rd ed., Springer, New York, 2017.

[7] S. I. KABANIKHIN, K. K. SABELFELD, N. S. NOVIKOV, AND M. A. SHISHLENIN, *Numerical solution of the multidimensional Gelfand-Levitan equation*, J. Inverse Ill-Posed Probl., 23 (2015), pp. 439–450.

[8] S. I. KABANIKHIN, A. D. SATYBAEV, AND M. A. SHISHLENIN, *Direct Methods of Solving Inverse Hyperbolic Problems*, VSP, Utrecht, Netherlands, 2005.

[9] V. A. KHOA, G. W. BIDNEY, M. V. KLIBANOV, L. H. NGUYEN, L. NGUYEN, A. SULLIVAN, AND V. N. ASTRATOV, *Convexification and experimental data for a 3D inverse scattering problem with the moving point source*, Inverse Problems, to appear.

[10] M. V. KLIBANOV, *Carleman estimates for the regularization of ill-posed Cauchy problems*, Appl. Numer. Math., 94 (2015), pp. 46–74.

[11] M. V. KLIBANOV, *Convexification of restricted Dirichlet to Neumann map*, J. Inverse Ill-Posed Probl., 25 (2017), pp. 669–685.

[12] M. V. KLIBANOV, *On the travel time tomography problem in* 3*D*, J. Inverse Ill-Posed Probl., 27 (2019), pp. 591–607.

[13] M. V. KLIBANOV, *Travel time tomography with formally determined incomplete data in 3D*, Inverse Probl. Imaging, 13 (2019), pp. 1367–1393.

[14] M. V. Klibanov, A. E. Kolesov, L. Nguyen, and A. Sullivan, *A new version of the convexification method for a 1-D coefficient inverse problem with experimental data*, Inverse Problems, 34 (2018), 35005.
[15] M. V. Klibanov, J. Li, and W. Zhang, *Convexification of electrical impedance tomography with restricted Dirichlet-to-Neumann map data*, Inverse Problems, 35 (2019), 035005.
[16] M. V. Klibanov and L. H. Nguyen, *PDE-based numerical method for a limited angle X-ray tomography*, Inverse Problems, 35 (2019), 045009.
[17] M. V. Klibanov, L. H. Nguyen, and K. Pan, *Nanostructures imaging via numerical solution of a 3-d inverse scattering problem without the phase information*, Appl. Numer. Math., 110 (2016), pp. 190–203.
[18] M. V. Klibanov and V. G. Romanov, *Reconstruction procedures for two inverse scattering problems without the phase information*, SIAM J. Appl. Math., 76 (2016), pp. 178–196.
[19] R. Lattès and J. L. Lions, *The Method of Quasireversibility: Applications to Partial Differential Equations*, Elsevier, New York, 1969.
[20] T. T. Le and L. H. Nguyen, *A convergent numerical method to recover the initial condition of nonlinear parabolic equations from lateral Cauchy data*, J. Inverse Ill-Posed Probl., https://doi.org/10.1515/jiip-2020-0028 (2020).
[21] Q. Li and L. H. Nguyen, *Recovering the initial condition of parabolic equations from lateral Cauchy data via the quasi-reversibility method*, Inverse Probl. Sci. Eng., 28 (2020), pp. 580–598.
[22] F. Monard, *Numerical implementation of geodesic X-ray transforms and their inversion*, SIAM J. Imaging Sci., 7 (2014), pp. 1335–1357.
[23] R. G. Mukhometov, *The reconstruction problem of a two-dimensional Riemannian metric and integral geometry*, Soviet Math. Dokl., 18 (1977), pp. 32–35.
[24] R. G. Mukhometov and V. G. Romanov, *On the problem of determining an isotropic Riemannian metric in the n-dimensional space*, Dokl. Acad. Sci. USSR, 19 (1978), pp. 1330–1333.
[25] L. H. Nguyen, Q. Li, and M. V. Klibanov, *A convergent numerical method for a multi-frequency inverse source problem in inhomogenous media*, Inverse Probl. Imaging, 13 (2019), pp. 1067–1094.
[26] L. Pestov and G. Uhlmann, *Two dimensional simple Riemannian manifolds are boundary distance rigid*, Ann. Math., 161 (2005), pp. 1093–1110.
[27] V. G. Romanov, *Integral geometry on isotropic Riemannian metric*, Dokl. Akad. Nauk SSSR, 241 (1978), pp. 290–293.
[28] V. G. Romanov, *Inverse Problems of Mathematical Physics*, VNU Press, Utrecht, Netherlands, 1986.
[29] V. G. Romanov, *Problem of determining the permittivity in the stationary system of Maxwell equations*, Dokl. Math., 93 (2017), pp. 1–5.
[30] U. Schrőder and T. Schuster, *An iterative method to reconstruct the refractive index of a medium from time-off-light measurements*, Inverse Problems, 32 (2016), 085009.
[31] J. A. Sethian, *Level Set Methods and Fast Marching Methods: Evolving Interfaces in Computational Geometry, Fluid Mechanics, Computer Vision, and Materials Science*, Cambridge Monogr. Appl. Comput. Math., Cambridge University Press, Cambridge, 1999.
[32] A. V. Smirnov, M. V. Klibanov, and L. H. Nguyen, *On an inverse source problem for the full radiative transfer equation with incomplete data*, SIAM J. Sci. Comput., 41 (2019), pp. B929–B952.
[33] P. Stefanov, G. Uhlmann, and A. Vasy, *Local and Global Boundary Rigidity and the Geodesic X-Ray Transform in the Normal Gauge*, https://arxiv.org/abs/1702.03638v2, 2017.
[34] P. Stefanov, G. Uhlmann, and A. Vasy, *Inverting the local geodesic X-ray transform on tensors*, J. Anal. Math., 136 (2018), pp. 151–208.
[35] L. Volgyesi and M. Moser, *The inner structure of the Earth*, Period. Polytech. Chem. Eng., 26 (1982), pp. 155–204.
[36] E. Wiechert and J. Zoeppritz, *Uber Erdbebenwellen*, Nachr. Koenigl. Ges. Wiss. Göttingen, 4 (1907), pp. 415–549.
[37] B. N. Zakhariev and A. A. Suzko, *Potentials in Quantum Scattering. Direct and Inverse Problems*, Energoatomizdat, Moscow, 1985.
[38] H. Zhao and Y. Zhong, *A hybrid adaptive phase space method for reflection travel time tomography*, SIAM J. Imaging Sci., 12 (2019), pp. 28–53.